Formation and evolution of Newton's regions of convergence in some problems of Celestial Mechanics

Tilemahos J. Kalvouridis and Irene T. Kalvouridis

National Technical University of Athens

Faculty of Applied Sciences, Department of Mechanics

Abstract

In nonlinear dynamical problems, chaos appears in many aspects of their investigation. In this paper we show the chaotic character of the regions of convergence as it is resulted from the numerical investigation of the equilibrium points in some known problems of Celestial Dynamics.

Keywords: chaos; regions of convergence; equilibrium points; Celestial Mechanics; Newton's algorithm.

1 Introduction

One of the most important steps in the study of a dynamical problem is the determination of the equilibrium states of the system. In nonlinear problems this is achieved by using numerical methods. During this process, the nonlinearity of a problem reveals some chaotic aspects of the problem that, beyond the very impressive pictures it provides, it also has some practical benefits. This is exactly the aim of this paper; to give information about the way that the regions of convergence are formed and evolve, in various problems of Celestial Mechanics. Furthermore, we investigate their parametric variation and we establish various general rules and remarks. This issue has been discussed in various papers that have been appeared the last few years ([1]-[6]). For our purposes we have selected the well known Newton's method, which is simple, popular, efficient, fast and accurate. For applications we have selected some known problems of Celestial Mechanics, such as the restricted three-body problem, the gravitational regular-polygon problem of $(N + 1)$ bodies, the photo-gravitational Copenhagen problem, the restricted five-body problem of Ollöngren, the Marañhao-Llibre problem of $3 + 1$ bodies and the ring problem of $N + 1$ bodies with radiation pressure. In all these problems or versions, we study the planar

motion of a very small body in the force field created by $N > 1$ big bodies (primaries) of the dynamical system.

2 Description of the considered cases, equations of planar motion of the small particle and potential functions

2.1 General characteristics and equations of motion

In all the above cases, a small body (or a particle) moves in the force field created by two or more, much bigger bodies, the primaries. This force field can be either purely gravitational or a combination of a gravitational one and a field coming from one or more radiating primaries. If we consider that the primaries, in all these cases, rotate with constant angular velocity around their center of mass, then the motion of the small body in a synodic coordinate system, which is rigidly attached to the rotating primaries, is described in normalized quantities by the following set of second order differential equations,

$$\ddot{x} - 2\dot{y} = \frac{\partial U}{\partial x}, \qquad \ddot{y} + 2\dot{x} = \frac{\partial U}{\partial y} \tag{1}$$

where $U(x, y)$ is the potential function, that has a different form in each of the considered cases. From the above equations we obtain a Jacobian-type integral of motion

$$\dot{x}^2 + \dot{y}^2 = 2\Omega(x, y) - C \tag{2}$$

where C is the so-called Jacobian constant.

2.2 Case 1: The restricted three-body problem

The well-known restricted three-body problem deals with the motion of a small particle in the gravitational field produced by two major bodies called the primaries, P_1 and P_2 that rotate around their center of mass in circular orbits with constant angular velocity (here considered as 1)(Figure 1a). It is characterized by one parameter μ which is the reduced mass $m_2/(m_1 + m_2)$ of primary P_2. The potential function U in this case has the form,

$$U = \frac{1}{2}\left(x^2 + y^2\right) + \frac{1 - \mu}{r_1} + \frac{\mu}{r_2} + \frac{1}{2}\mu(1 - \mu) \tag{3}$$

r_1 and r_2 are the distances of the small body from the two primaries, with

$$r_1^2 = (x - \mu)^2 + y^2, \qquad r_2^2 = (x - \mu + 1)^2 + y^2.$$
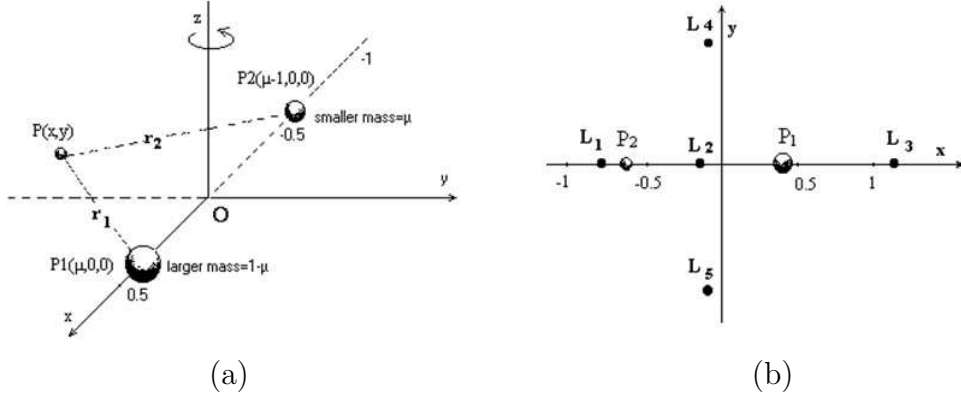
(a)   (b)

Figure 1.— (a) The configuration of the restricted three-body problem and the synodic coordinate system (b) The distribution of the equilibrium points

2.3   Case 2: The photo-gravitational Copenhagen problem

The Copenhagen problem is a particular case of the restricted three-body problem with $\mu = 0.5$ (Figure 2a). Here, we consider that in addition to their gravitational character, the primaries are also radiating sources with radiation coefficients q_1 and q_2 respectively. Therefore the problem depends on two parameters namely q_1 and q_2. In this case the potential function has the form

$$U(x,y) = \frac{1}{2}\left[\left(x^2 + y^2\right) + \sum_{i=1}^{2}\frac{q_i}{r_i}\right] \tag{4}$$

$$r_1 = \left[\left(x - \frac{1}{2}\right)^2 + y^2\right]^{1/2}, \qquad r_2 = \left[\left(x + \frac{1}{2}\right)^2 + y^2\right]^{1/2}$$

r_1 and r_2 are the distances of the particle from the primaries

$$q_i = 1 - b_i, \quad i = 1, 2, \quad \text{where } b = \frac{F_r}{F_g} \tag{5}$$

are, for each radiating source, the ratios of force F_r caused by radiation, to force F_g caused by gravitation.

2.4   Case 3: The gravitational regular polygon problem of $N + 1$ bodies

The regular polygon problem of $(N+1)$ bodies, deals with the motion of a small body in the combined Newtonian field created by N much bigger bodies called the primaries. $\nu = N - 1$ of these have equal masses m and are arranged at the vertices of a regular ν-gon while the Nth primary is located at the center of mass of the configuration (Figure 3). The peripheral primaries rotate about their center of mass with the same constant angular velocity. The system is characterized by two parameters: the mass parameter $\beta = m_0/m$, that is the ratio of the central mass m_0 to a peripheral one, and the number ν of the peripheral primaries.
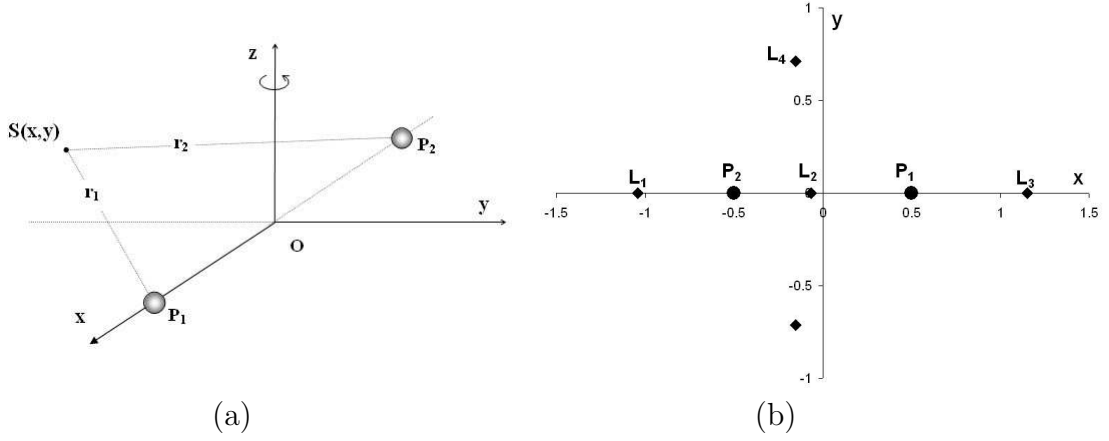
(a)   (b)

Figure 2.— The photogravitational Copenhagen case. (a) The configuration of the system. (b) Distribution of the equilibria of the small body when $b_1 = 0.1$, $b_2 = 0.5$
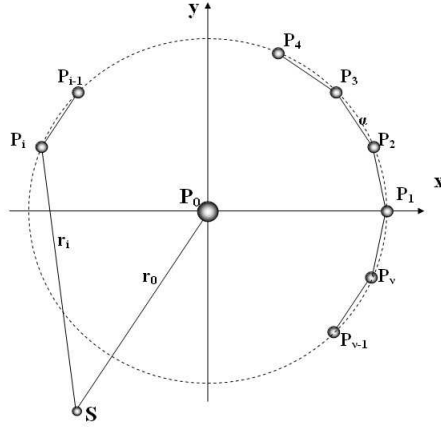

Figure 3.— The planar ring problem of $(N + 1)$ bodies

$$U(x, y) = \frac{1}{2} \left(x^2 + y^2 \right) + \frac{1}{\Delta} \left[\frac{\beta}{r_0} + \sum_{i=1}^{\nu} \frac{1}{r_i} \right] \tag{6}$$

$$\Delta = 2 \sin \theta \left[\sum_{i=2}^{\nu} \frac{\sin^2 \theta}{\sin(i-1)\theta} + 4\beta \sin^2 \theta \right], \quad \theta = \pi/\nu \tag{7}$$

and

$$r_0 = \left(x^2 + y^2 \right)^{1/2}, \quad r_i = \left[(x_i - x)^2 + (y_i - y)^2 \right]^{1/2}, \quad i = 1, 2, 3, \ldots, \nu$$

are respectively the distances of the particle from the central primary and the peripheral ones, where x_i and y_i are their coordinates. The equilibrium locations are arranged on either five or three circular zones depending on the value of the mass parameter β. If this parameter is less than a critical value l_ν (different for each configuration) then five zones exist (Figure 4a). Otherwise, three equilibrium zones are formed (Figure 4b).
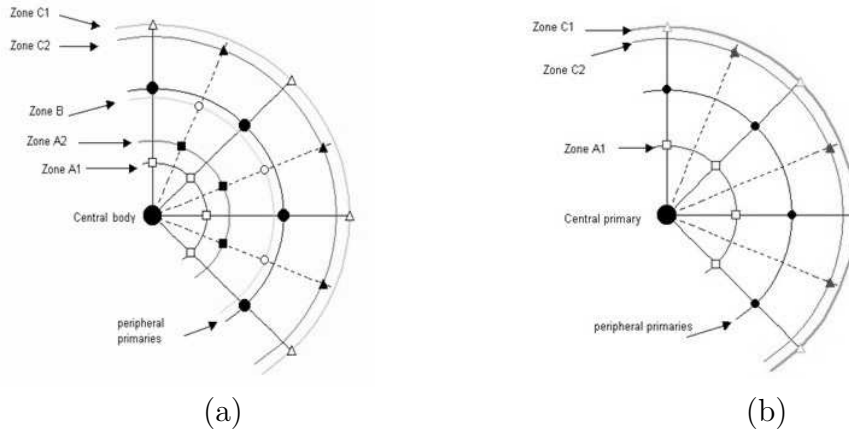
56

(a)   (b)

Figure 4.— General distribution of the equilibrium positions in the ring problem of
$N + 1$ bodies for two cases: (a) $\beta < l_\nu$, (b) $\beta > l_\nu$, (l_ν is the critical value of the mass
parameter)

2.5   Case 4: The restricted five-body problem of Ollöngren

Three big bodies P_1, P_2, P_3 with equal masses m are located at the vertices of an
imaginary equilateral triangle. A fourth body P_0 with mass m_0 is located at the mass
center of the system. A small particle S with negligible mass moves in the resultant force
field of the big bodies (Figure 5). The system is characterized by one parameter which is
the ratio $\beta = m_0/m$ of the central mass to a peripheral one. The configuration has three
axes of symmetry since it is identified after a rotation of 120° around the perpendicular
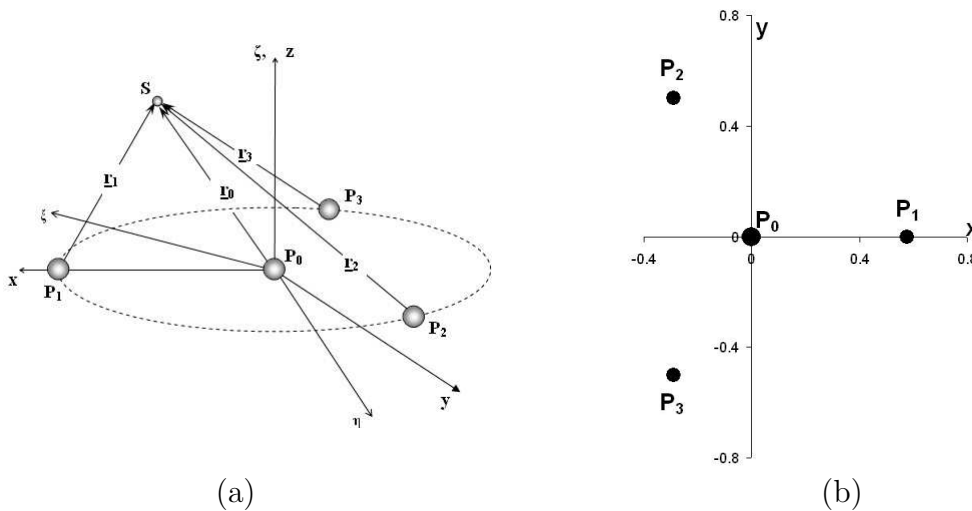axis Oz. The potential function has the form,

(a)   (b)

Figure 5.— The five-body problem of Ollöngren. (a) The three-dimensional case, (b)
the planar configuration of the primaries

$$U = \frac{1}{2}\left(x^2 + y^2\right) + \frac{1}{3(1 + \beta\sqrt{3})}\left[\frac{\beta}{r_0} + \sum_{i=1}^{3}\frac{1}{r_i}\right] \tag{8}$$

57

where

$$r_0 = \left(x^2 + y^2\right)^{1/2}, \qquad r_i = \left[(x_i - x)^2 + (y_i - y)^2\right]^{1/2}.$$

The small body S has fifteen equilibrium locations when $\beta < 0.014$. They are grouped in five groups, A_1, A_2, B, C_2 and C_1 by order of appearance from the origin outwards. More specifically, the equilibria of groups A_1 and C_1 are located on the radii that join the central primary and the peripheral ones. Those of A_2, B and C_2 are located on the bisectors of the angles formed by two consecutive primaries and the central one (Figure 6a). The equilibria of each group have the same Jacobian constant C and are characterized by the same state of stability. When $\beta > 0.014$ six of these positions (groups A_2 and B) disappear and the system possesses only nine locations that belong to groups A_1, C_2 and C_1 (Figure 6b).
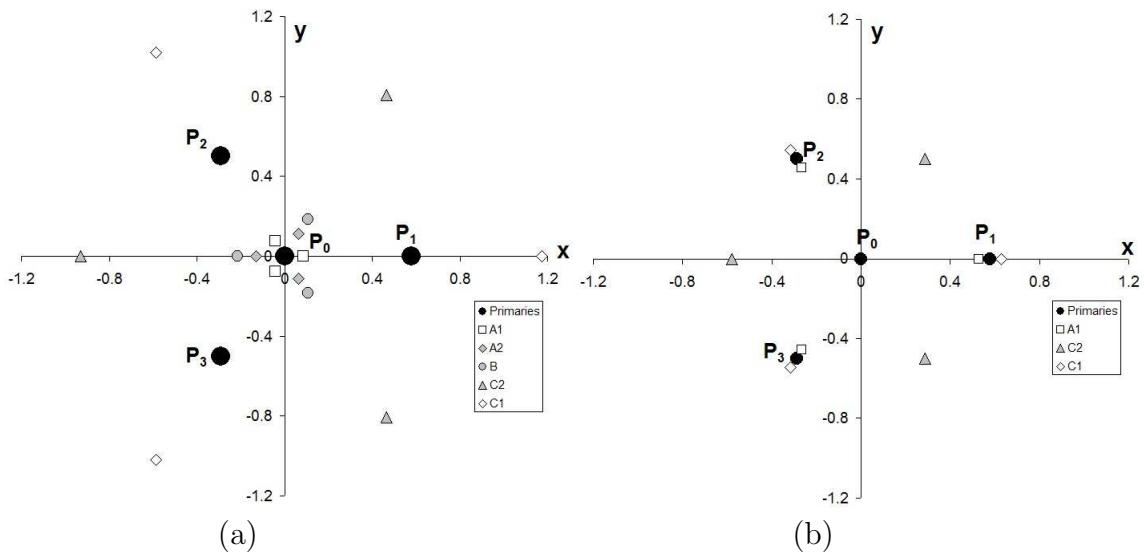

Figure 6.— Distribution of the equilibrium positions (a) for $\beta = 0.01$, (b) for $\beta = 500$

2.6 Case 5: The Marañhao-Llibre problem of $3 + 1$ bodies

The configuration is shown in Figure 7a. The problem is characterized by one parameter which is the mass ratio $\beta = m_0/m_1$. In this case the potential function has the form,

$$U = \frac{1}{2}\left(x^2 + y^2\right) + \frac{1}{2(1 + 4\beta)}\left[\frac{\beta}{r_0} + \sum_{i=1}^{2}\frac{1}{r_i}\right] \tag{9}$$

There are 6 equilibrium points for every value of parameter β $(\beta \neq 0)$. Two of them are disposed along the syzygies' axis (x-axis of the synodic coordinate system) in symmetric positions with respect to the origin O (group A_1). Two points lie on the same axis but beyond the peripheral primaries (group C_1). Finally, the remaining two points lie on the y-axis. They form a group which is symbolized by C_2. As the mass parameter decreases
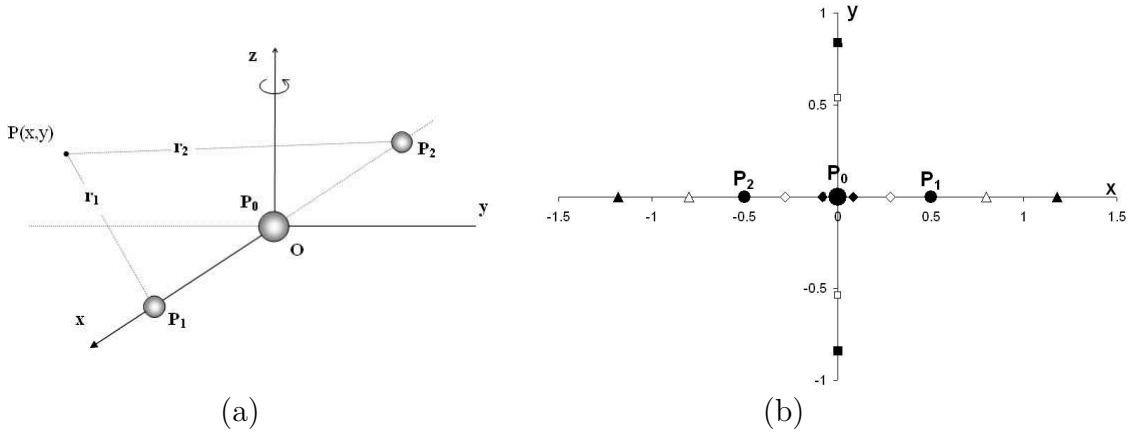
Figure 7.— The Marañhao-Llibre problem. (a) The configuration. (b) Distribution of the equilibrium positions (for $\beta = 0.2$ (full black) and for $\beta = 2$ (framed black))

the inner collinear points approach each other by moving towards the origin, where they coincide when $\beta = 0$. On the contrary, the outer collinear points go away from each other and from the origin. As a consequence, for the limit value $\beta = 0$, we obtain the five Lagrange equilibrium positions of the Copenhagen case of the restricted three-body problem. Figure 7b shows the distribution of the equilibrium points for $\beta = 0.2$ and $\beta = 2$.

2.7 Case 6: The photo-gravitational ring problem of $N + 1$ bodies

The arrangement of the primaries is the same as in the gravitational version. However, one or more primaries are radiation sources and therefore the system in the general case is characterized by $N + 2$ parameters, that is the number ν of the peripheral bodies, the mass parameter β and the $N = \nu + 1$ radiation coefficients b_i, $i = 0, \ldots, \nu$. The symmetries that appear in the gravitational case are generally destroyed and only in the three following cases is preserved:

(a) The central body is a radiation source (whatever the value of the radiation coefficient b_0 is).

(b) All peripheral bodies are radiation sources and have the same radiation coefficients.

(c) All the primaries are radiation sources and the peripheral bodies have the same radiation coefficients.

The potential has the form,

$$U = \frac{1}{2}\left(x^2 + y^2\right) + \frac{1}{\Delta}\left[\frac{\beta q_0}{r_0} + \sum_{i=1}^{\nu} \frac{q_i}{r_i}\right] \tag{10}$$

where Δ is the same as in the gravitational case (relation (7)) and q_i are the radiation parameters that are given by relations (5). The number of the existing equilibrium points depends on the values of the N radiation coefficients. In all cases where the symmetry that

exists in the gravitational case, is preserved, the configuration has 2ν axes of symmetry and the equilibria are located along them. The equilibrium positions are assembled either in five or three groups of ν points each. Figure 8 shows the distribution of the equilibrium locations for two cases where symmetry is preserved. In Figure 8a all primaries radiate with the same radiation coefficients $b = 0.5$, while in Figure 8b all peripheral primaries radiate with the same radiation coefficients $b = 0.9$.
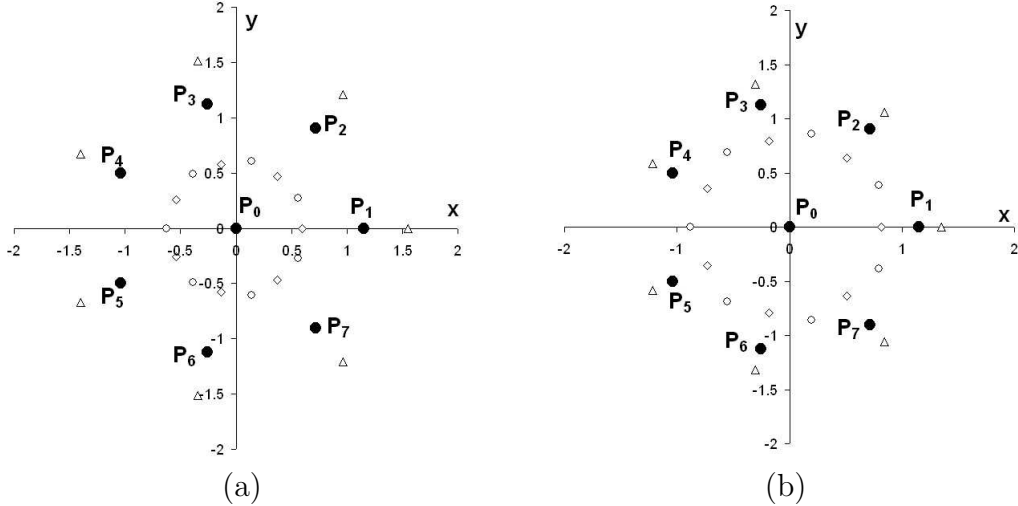

Figure 8.— Distribution of the equilibrium locations in the photo-gravitational ring problem when $\nu = 7$, $\beta = 2$. We mark with small triangles the equilibria of group C_1, with small circles the equilibria of group A_2 and with small rhomboids the equilibria of group A_1. (a) All primaries radiate with radiation coefficients $b = 0.5$ (b) All peripheral primaries radiate with radiation coefficients $b = 0.9$

3   The numerical method and some preliminary notes

3.1   Conditions for equilibrium

The conditions for an equilibrium position of the small body, are $\dot{x} = \dot{y} = \ddot{x} = \ddot{y} = 0$. Under these conditions, these locations are the solutions of the nonlinear system of algebraic equations

$$\frac{\partial U}{\partial x} = 0, \qquad \frac{\partial U}{\partial y} = 0. \tag{11}$$

To locate the equilibrium points on the plane (x, y) we apply a numerical method to solve equations (11).

3.2   The equivalence principle of the equilibrium points

In any dynamical system if two or more equilibrium positions have exactly the same dynamical properties, which means, the same energy (here the value of the Jacobian

constant C) and the same state of stability, then are dynamically equivalent. This property is usually dictated by the symmetry of the force field created by the members of the system. For example the triangular equilibrium points L_4 and L_5 in the restricted three-body problem are dynamically equivalent for any value of the mass parameter μ. When $\mu = 0.5$ (Copenhagen gravitational case) equilibrium points L_1 and L_3 are also dynamically equivalent. Furthermore, in the ring gravitational problem of $N+1$ bodies, the equilibrium points that belong to some particular equilibrium zone (A_1, A_2, B, C_2, C_1) are dynamically equivalent.

3.3 The crooked path described by the consecutive iterations of the numerical method

We can describe the consecutive iterations of the numerical algorithm as the "motion" of a "point" on a crooked path, just like the Brownian motion of an atom of a gas.
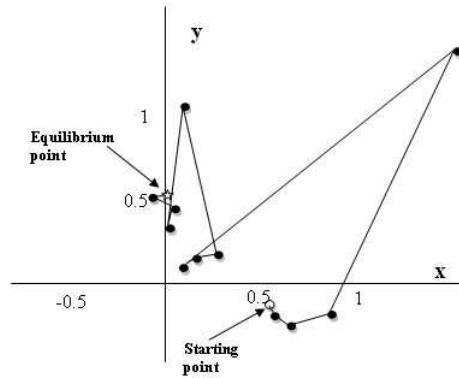

Figure 9.— The crooked path formed by the consecutive approximations of the numerical method

3.4 Sensitivity to small changes in the initial values

The term sensitivity at this point is used to describe the way that the path followed by the method during the iterative process, is affected by small perturbations to the initial values. This sensitivity is evinced by various ways. Here we show five of them:

(1) A small change of the initial values leads to the same equilibrium position with the same or almost the same number of steps.

(2) A small change of the initial values leads to the same equilibrium position but the number of steps significantly differs from the one in the unperturbed case (Figure 10a).

(3) A small change of the initial values leads to a different equilibrium position (dynamically equivalent or not) of the system after a number of steps (Figure 10b).

(4) A small change of the initial values leads to a non-convergent state (Figure 10c).

(5) A small change of the initial values leads to a state in which the "point" oscillates between two values and never reaches the target (Figure 10d).
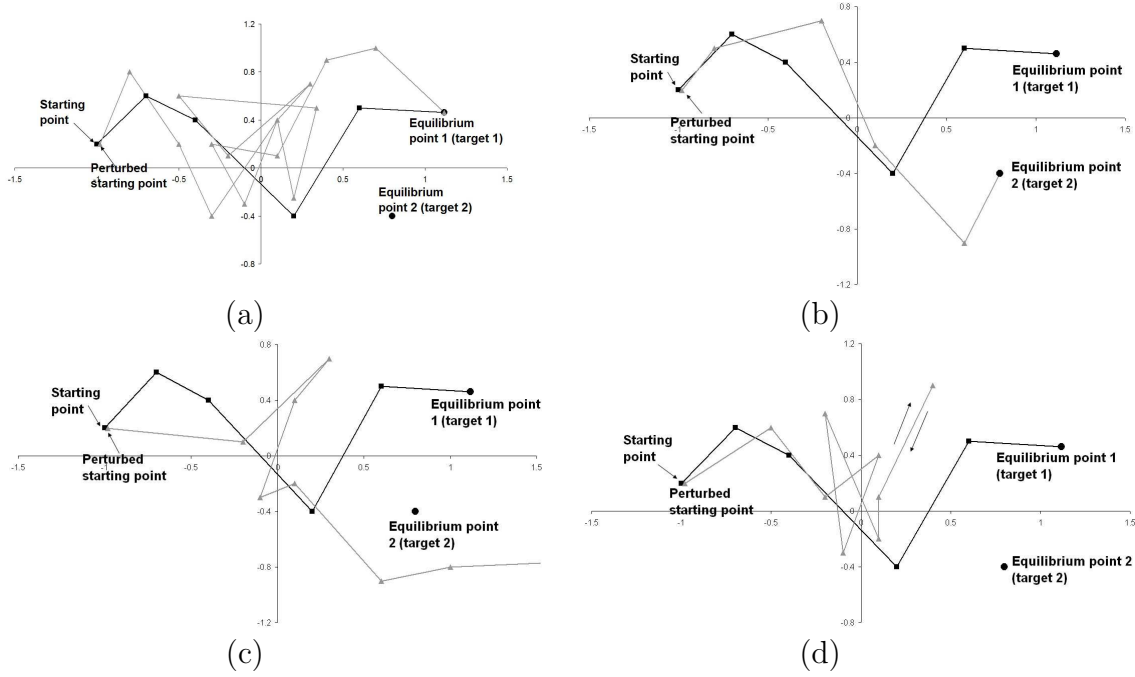
(a)   (b)

(c)   (d)

Figure 10.— The black lines show the "unperturbed" paths and the gray lines the "perturbed" ones; (a) the "perturbed" path reaches the same target as the "unperturbed" one but in a very different number of steps; (b) the "perturbed" path reaches a different target (equilibrium point); (c) the "perturbed" path dos not converge at all; (d) the "perturbed" path after some steps "oscillates" between two values

3.5 The numerical method

Several methods for solving algebraic systems of non linear equations are known. However, Newton's method still remains a fast (it converges quadratically), simple and accurate method. In the past (see [3] and [4]), we have used and compared post Newtonian methods like the Broyden's method and an improved version of it. Although the obtained results are qualitatively similar, however, those obtained from Newton's method seem to be much better. The Newton's algorithm for the general case of equations (11) takes the form,

$$
\begin{aligned}
x_n &= x_{n-1} - \left. \frac{U_x U_{yy} - U_y U_{xy}}{U_{yy} U_{xx} - U_{xy}^2} \right|_{(x_{n-1}, y_{n-1})} \\
y_n &= y_{n-1} + \left. \frac{U_x U_{yx} - U_y U_{xx}}{U_{yy} U_{xx} - U_{xy}^2} \right|_{(x_{n-1}, y_{n-1})}
\end{aligned}
\tag{12}
$$

where we symbolize with U_x, U_y, U_{xx}, U_{yy}, U_{xy} the first and second derivatives of U calculated at the $(n-1)$th step of the iteration process. The process terminates when some predetermined accuracy is reached.

4 The regions of convergence

4.1 General remarks and comments

The regions of convergence (or basins of convergence, or attracting domains) are formed by the launching points of the applied particular numerical method that lead to dynamically equivalent equilibrium positions of the system. As it is shown in the figures obtained from the various case-problems, each region has a fractal structure and generally consists of a "compact" area which evolves around an equilibrium location and of randomly dispersed points that are mixed with the dispersed points that belong to basins of other equilibrium points or equilibrium groups. Next we shall expose the results concerning these regions for each of the considered cases. In Cases 4, 5 and 6 (Figures 14 to 16) we also give the attracting sub-domains which are formed by considering the number of the steps that are needed to reach the equilibrium positions.

4.2 Case 1: The restricted three-body problem

Figure 11 shows the evolution of the regions of convergence for the five Lagrangian points.

The basin of convergence of L_1, occupies the smallest area of all the basins for every value of μ ($0 < \mu < 0.5$). It consists of two "compact" areas of limited extent and of dispersed points (Figure 11a). Both "compact" areas are developed on the left of primary P_2 and are symmetrically arranged with respect to the x-axis. As μ increases, the attracting region expands, while the "compact" regions widen and the dispersed points increase and become denser around the "compact" areas, thus forming fine fractal structures.

The region of convergence of point L_2 consists of two "compact" areas. The first one extends between the two primaries P_1 P_2, while the second one is extended beyond the "compact" regions of L_1 (Figure 11b). The dispersed points which belong to this basin form fractal boundaries. As μ augments the dispersed points become denser, thus forming fractal protrusions near the boundaries of the "compact" areas corresponding to the collinear Lagrangian points.

The region of convergence of L_3 is homothetic of $R(L_1)$ with homothetic ratio > 1. Its center of homothety is a point lying on the x-axis, close to L_2. As μ increases for $0 < \mu < 0.5$, the homothetic ratio approaches 1 and the center of homothety approaches equilibrium position L_2. The region of convergence of L_3 consists of two "compact" areas which extend on the right of primary P_1, as well as of numerous dispersed points (Figure 11c). It shrinks as μ augments.

The region of L_4 holds numerous "compact" areas that extend on the semi-plane $y > 0$. The dispersed points spread all over the plane (Figure 11d). As μ increases, this region
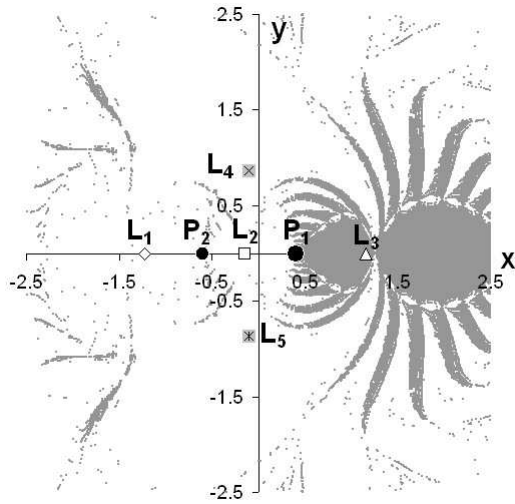
expands, the "compact" areas tend to unite, thus forming a great "compact" area, while the dispersed points become denser inside the area of the basin boundaries. Finally the basin of convergence of L_5 is symmetric with the one of L_4 as regards the x-axis and therefore presents exactly the same characteristics (Figure 11e).
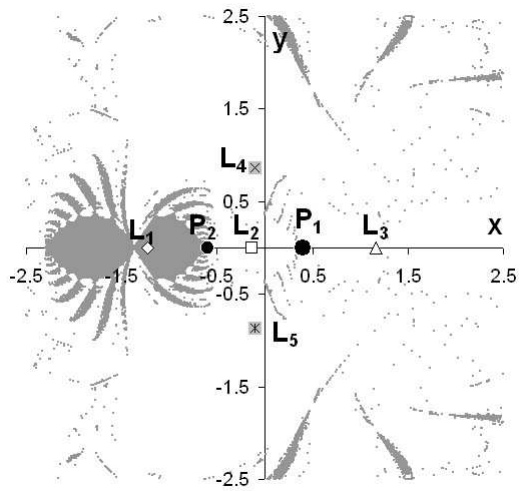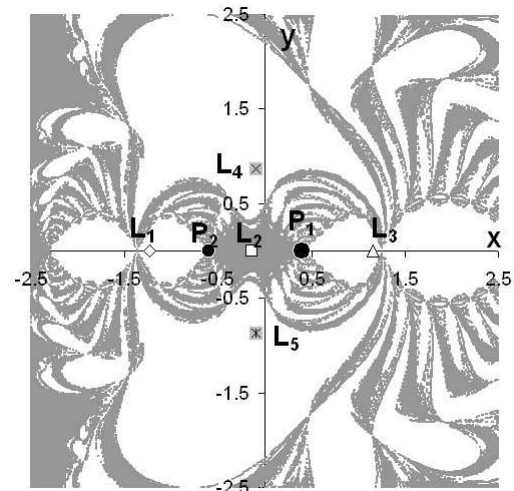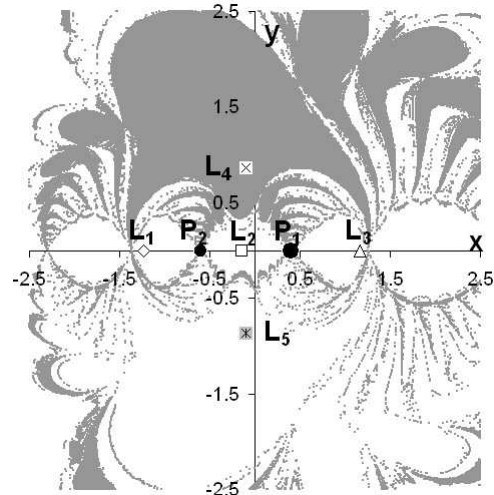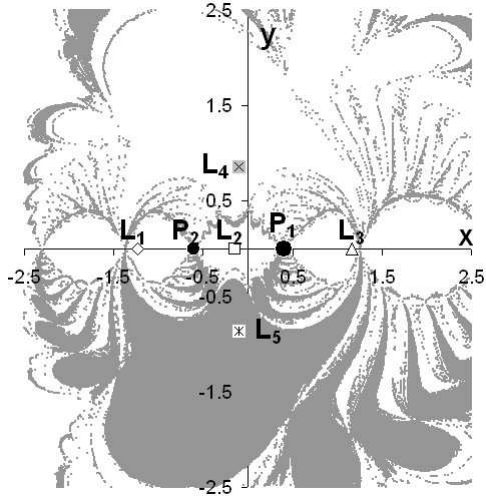

(a)   (b)

(c) (d)

(e)

Figure 11.— Restricted three-body problem; regions of convergence for $\mu = 0.4$. (a) L_1, (b) L_2, (c) L_3, (d) L_4, (e) L_5

4.3 Case 2: The photo-gravitational Copenhagen problem

In this problem the two primaries have equal masses and are both radiation sources. The primaries occupy the same relative distances in the synodic coordinate system. The radiation forces influence the small particle but they do not influence the motion of the primaries. In Figure 12 we can see the regions of convergence of the equilibria that evolve on the upper half of the xy-plane. The picture on the other half of the plane is symmetric with respect to the x-axis. We mark with D some sub-domains which consist of dispersed points and with S the "compact" regions.
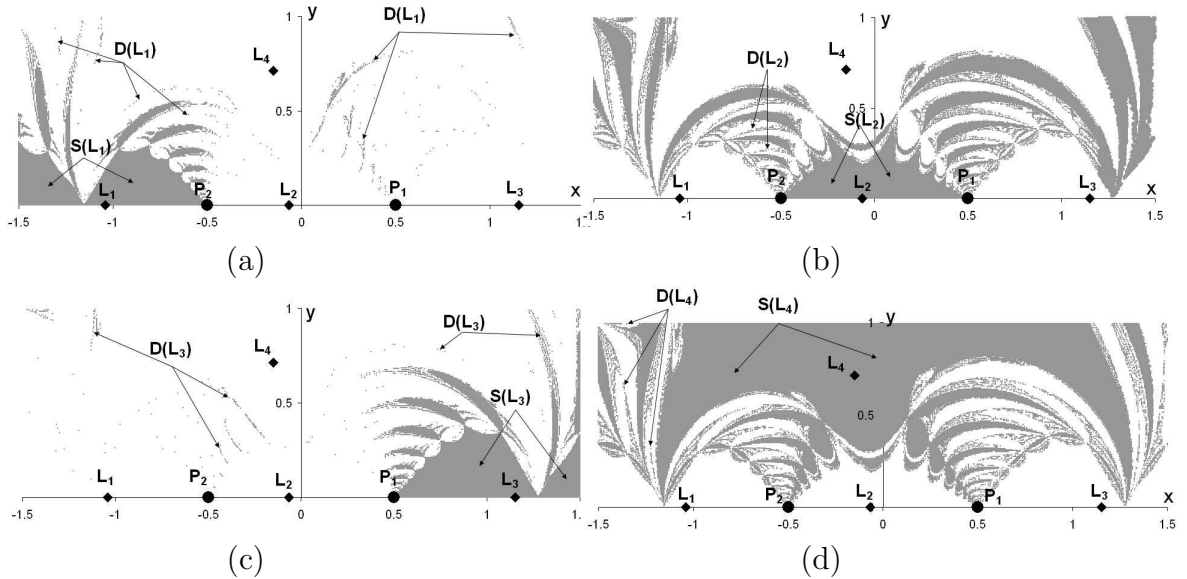
Figure 12.— Regions of convergence in the photo-gravitational Copenhagen problem for $b_1 = 0.1$, $b_2 = 0.5$; (a) L_1, (b) L_2, (c) L_3, (d) L_4

4.4   Case 3: The gravitational regular polygon problem of $N + 1$ bodies

As in the previous case, we mark with D the sub-domains which consist of the dispersed points and with S the "compact" regions. The boundaries of the latter regions are not clearly defined. Figure 13 shows a case with $N = 11$ (regular decagon) and $\beta = 12.5$ ($\beta > l_\nu$). As we have mentioned before, there are three equilibrium zones, A_1, C_2, C_1. The attracting domain of A_1 presents diamond-shaped "compact" parts, whose wavy sides have vague boundaries. These areas develop between the central primary and each of the peripheral ones (Figure 13a). The attracting area of C_1 generally consists of two basic "compact" regions, the biggest of which contains the equilibrium point (Figure 13b). As regards the dispersed points, on the one hand they are organized in a dense way around the two basic "compact" regions, and on the other hand, they are diffused at the boundaries of the "compact" regions of the other zones. In the plane areas that lie between the "compact" regions of A_1 and C_1 stretch the "compact" regions of the attracting area of C_2, (Figure 13c). The dispersed points surround densely the "compact" regions, but also diffuse at the boundaries of the compact regions of the other zones.
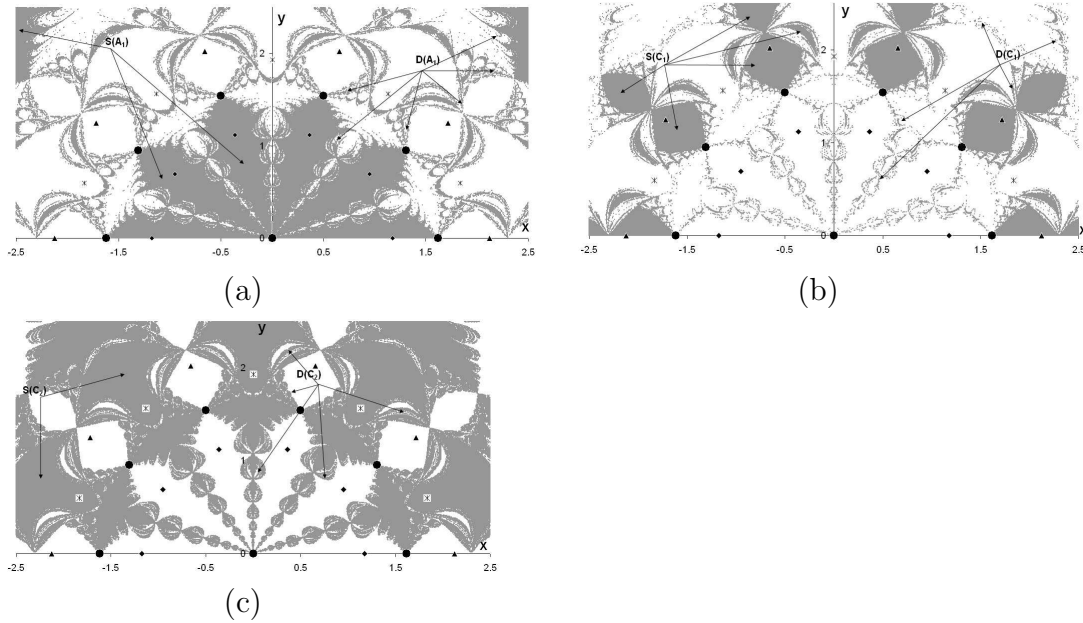
66

Figure 13.— Regions of convergence in the gravitational regular polygon problem of $N + 1$ bodies for $N = 11$ and $\beta = 12.5$; (a) zone A_1, (b) zone C_1, (c) zone C_2

4.5 Case 4: The restricted five-body problem of Ollöngren

The basins develop in the xy-plane in a way which is consistent with the symmetry of the primaries' configuration. In any case, the basin of group C_2 concentrates the majority of the considered launching points of the xy-plane, while that of group C_2 concentrates the minority of the points. Figure 14 shows two different cases for $\beta = 2$ and $\beta = 500$. As we can see, when β increases, the shape and size of these basins change; the basin of C_2 enlarges (Figures 14e and f) while those of A_1 and C_1 shrink (Figures 14a,b and 14c,d).
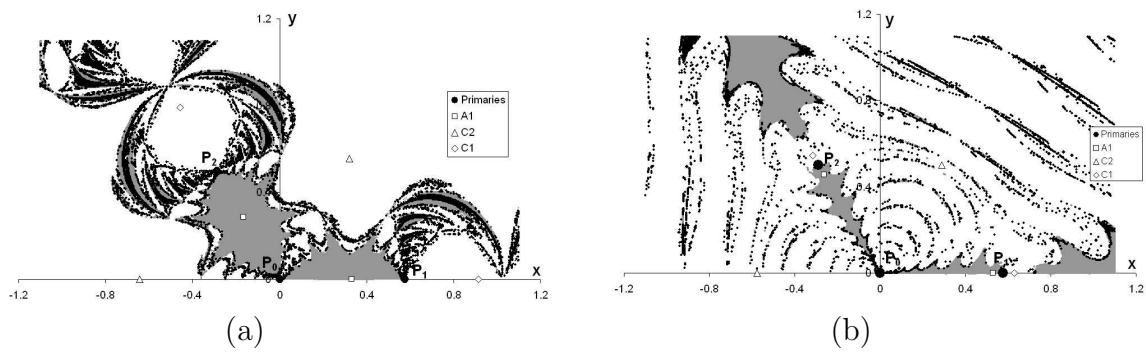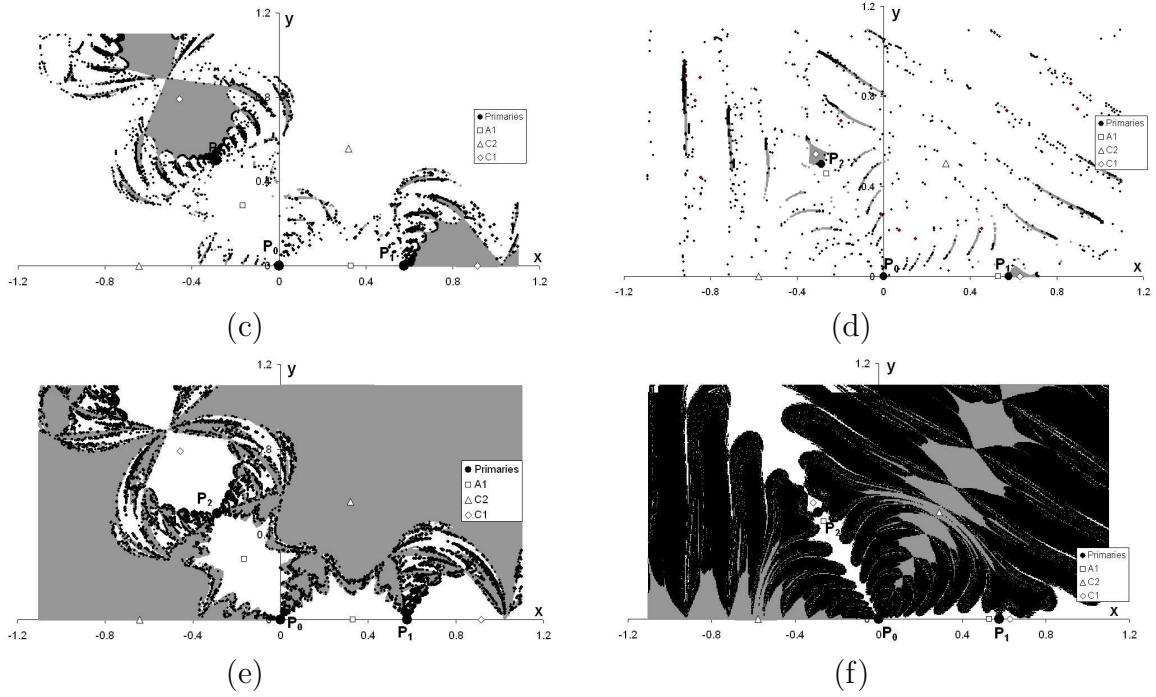
Figure 14.— Regions of convergence in the restricted five-body problem of Ollöngren. The gray regions consist of points where convergence occurs up to 9 iterations, while black regions consist of points where convergence occurs in more than 9 steps; (a) A_1 ($\beta = 2$), (b) A_1 ($\beta = 500$), (c) C_1 ($\beta = 2$), (d) C_1 ($\beta = 500$), (e) C_2 ($\beta = 2$), (f) C_2 ($\beta = 500$)

4.6 Case 5: The Marañhao-Llibre problem of $3 + 1$ bodies

Figure 15 shows the attracting domains of the three equilibrium groups for the value of the mass parameter, $\beta = 2$. A "deterministic" region with a fractal structure surrounds each equilibrium position of zone A_1. From its boundaries leap tentacles formed by dispersed points that terminate to the boundaries of the "compact" region of the symmetric equilibrium position of that group. Several other dispersed points also accumulate rather a long way from the x-axis in strip-like areas. Between these two concentrations no other points of this class exist (Figure 15a). When the mass parameter augments, then the "deterministic" regions shrink, while other similar areas are formed in a distance from the first ones. Regarding the attracting domain of zone C_2, it is the biggest one in comparison to the respective regions of the other two groups, as is evident in Figure 15c. It covers most of the surface of the xy plane but presents considerable gaps near the x-axis. As mass parameter β increases, the attracting domain extends and comes closer to the x-axis. The attracting domain of zone C_1 consists of four "deterministic" regions that are symmetrically disposed with respect to the origin. These regions are also symmetric with respect to the x-axis. Two of them, those that are closer to the origin, are wider than the other two. The dispersed points either form tentacles that come out from the boundaries

of the "deterministic" regions, or they form shapes that surround the origin and resemble the wings of a windmill (Figure 15b).
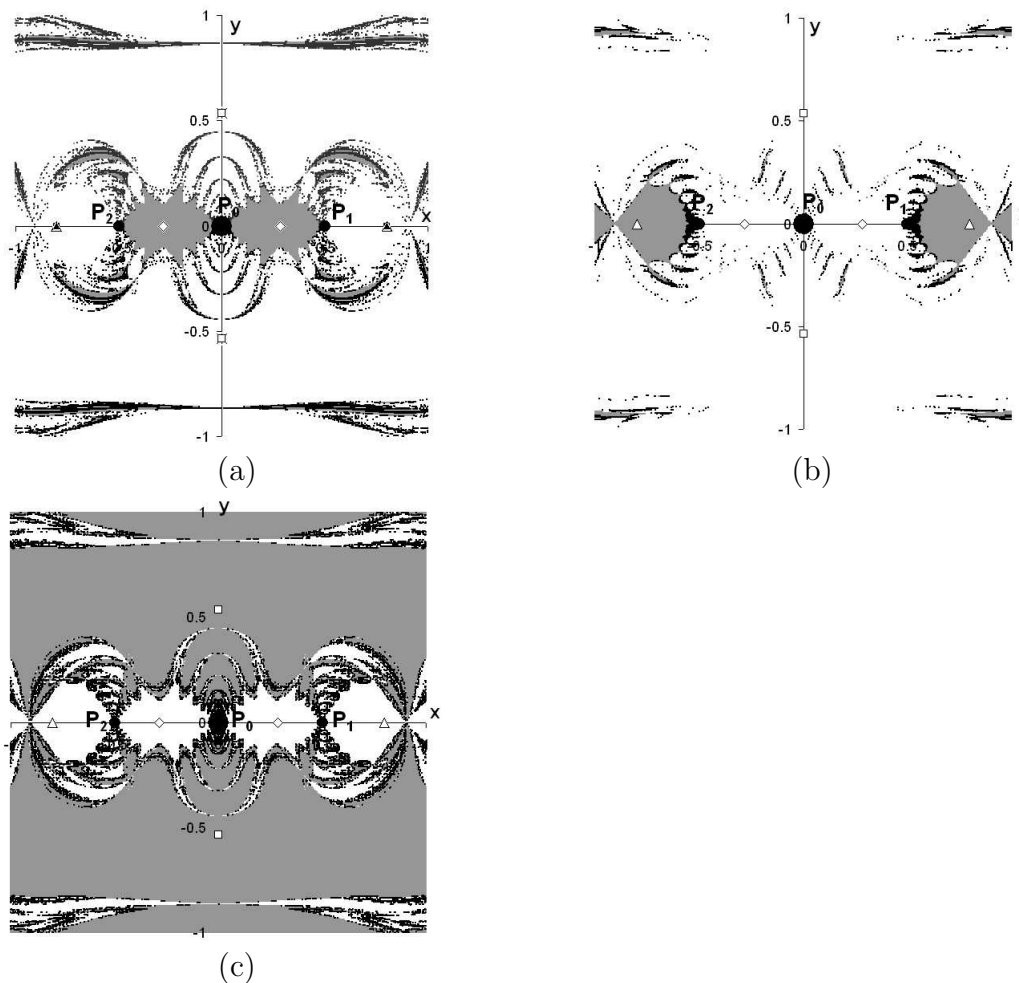

(a)

(b)

(c)

Figure 15.— Regions of convergence in the Marañhao-Llibre problem of $3 + 1$ bodies for $\beta = 2$; (a) zone A_1, (b) zone C_1, (c) zone C_2. The gray regions consist of points where convergence occurs up to 9 iterations, while black regions consist of points where convergence occur in more than 9 steps

4.7 Case 6: The photo-gravitational ring problem of $N + 1$ bodies

The domain of each basin presents, as it is expected, all the symmetry elements of the force field. The very dense parts mainly evolve around the equilibrium points of a given group, while the dispersed points lie on the boundaries of the dense regions of this group or other ones showing a chaotic aspect. The boundaries of the dense parts are not clear and in some cases present a fractal structure. Figure 16 shows a case in a configuration with $\nu = 7$ and $\beta = 2$, where all peripheral primaries are radiation sources with radiation coefficients 0.9. The points of each attracting region have been classified in three classes according to the number of iterations that are needed to achieve convergence with a

predetermined accuracy. The light gray regions consist of points characterized by very fast convergence ($1 - 5$ iterations) while the gray and the black regions are characterized by fast ($6 - 10$ iterations) or moderate convergence (more than 10 iterations) respectively. The sub-region of the first class is a very small one and evolves around each equilibrium position of this particular group. The sub-region of class interval $6 - 10$ iterations of each group consists of areas or points that mainly surround and complement the central regions of the first class interval. Regarding the region of class interval > 10 iterations, it merely consists of dispersed points lying either on the boundaries of the dense regions of the previously mentioned class interval, or between the dense regions of the other equilibrium groups.
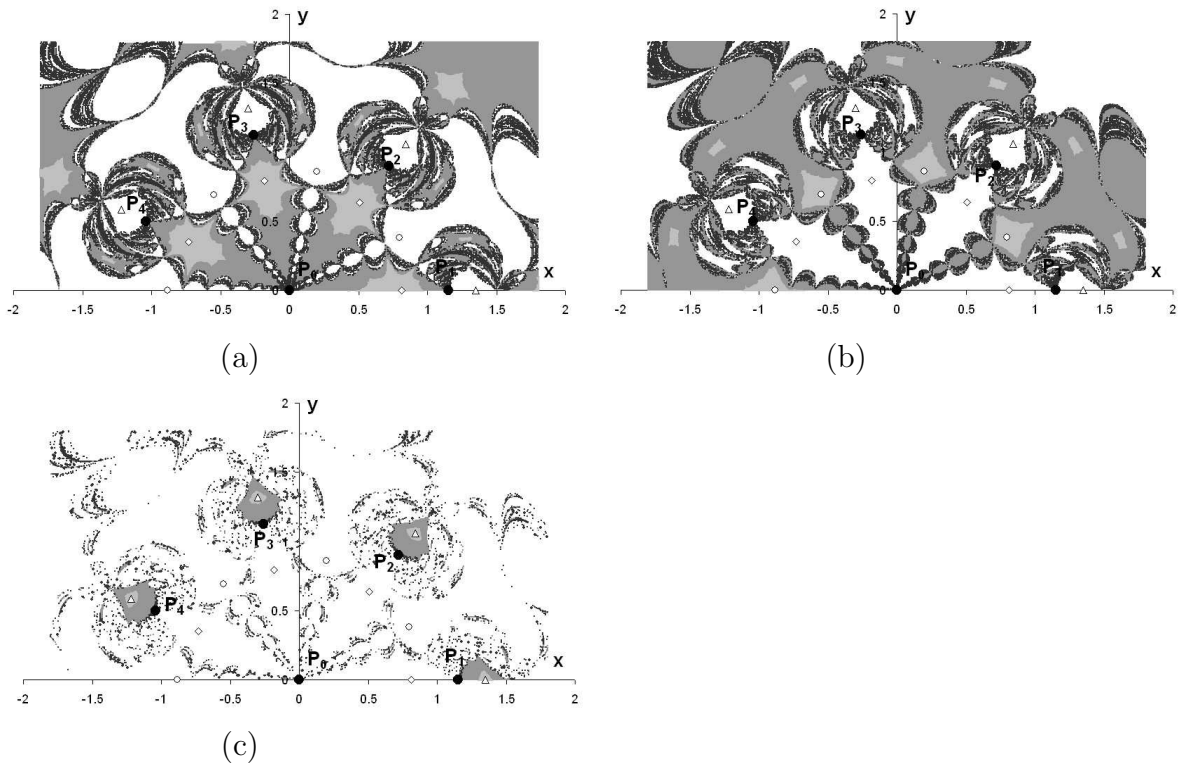

(a) (b)

(c)

Figure 16.— Regions of convergence in the photo-gravitational ring problem of $(N+1)$-bodies with $\nu = 7$ and $\beta = 2$, when all peripheral primaries are radiation sources with radiation coefficients 0.9; (a) A_1, (b) A_2, (c) C_1. (class $1 - 5$ steps (light gray), class $6 - 10$ steps (gray), class > 11 steps (black))

5   Conclusions and remarks

An attracting domain consists of "compact" parts and of dispersed points. These points are distributed on the boundaries of the compact parts of the same or other equilibrium points or zones. The central parts of the "compact" areas show a deterministic aspect, while in the areas where isolated points of different classes of iterations are mixed,

the chaotic character is obvious. The regions that consist of points which converge very fast to an equilibrium position, have "compact" parts which surround these positions and dispersed points. The "compact" parts do not have well defined boundaries. Regarding the regions of moderate or slow convergence, they merely consist of dispersed points lying either on the boundaries of the dense regions of the previously mentioned class interval, or between the dense regions of the other equilibrium points or groups. In all the examined cases the attracting domains present similar properties. The parameters that characterize each case (mass parameter, radiation coefficients, reduced mass, etc.) play an important role on the formation of these domains and they influence in a very definitive way their form and evolution, the distribution of their points on the working plane, as well as, their density and fractal structure.

References

[1] Croustalloudi, M., Kalvouridis, T.: 2007, *Attracting Domains in Ring-Type N-Body Formations*, Planet. Space Sci., **55**, 1-2, 53-69.

[2] Croustalloudi M., Kalvouridis T.: 2004, *Structure and parametric evolution of the Basins of attraction in the restricted three-body problem*, 7th National Congress on Mechanics, HSTAM, June 24-26, Technical Univ. of Crete, Chania, Crete, Greece, Vol. II, pp. **144-150**.

[3] Gousidou-Koutita, M., Kalvouridis, T.J.: 2008, *Numerical study of the attracting domains in a non-linear problem of Celestial Mechanics*, In: G. Akrivis, E. Gallopoulos, A. Hadjidimos, I. Kotsireas, D. Noutsos, M. Vrahatis (eds.) "Recent Approaches to Numerical Analysis: Theory, Methods and Applications", Proceedings, vol. 1, pp.**84-87**, (Conference in Numerical Analysis (NumAn2008), Kalamata, Greece, 1-5 September 2008).

[4] Gousidou-Koutita,M., Kalvouridis, T.J.: 2008, *On the efficiency of Newton and Broyden numerical methods in the investigation of the regular polygon problem of $(N + 1)$ bodies*, Appl.Math.Comp., 212 (2009), **100-112**.

[5] Kalvouridis, T.J., Paraskevopoulou, M.: 2009, *Basins of convergence in the restricted five-body problem of Ollöngren*, 2nd Chaotic Modeling and Simulation International Conference (CHAOS2009), 1-5 June 2009, Chania, Crete, Greece. ook of abstracts p. **31**.

[6] Douskos, Ch.: 2010, *Collinear equilibrium points of Hill's problem with radiation and oblateness and their fractal basins of attraction*, Astrophys. Sp. Sci., DOI: 10.1007/s10509-009-0213-5 (in press).